AERODYNAMIC PERFORMANCE OF A VERY-HIGH-LIFT LOW-PRESSURE TURBINE AIRFOIL (T106C) AT LOW REYNOLDS AND HIGH MACH NUMBER INCLUDING THE EFFECT OF INCOMING PERIODIC WAKES

J. Clinckemaillie[1] – L. Fattorini – T. Fontani – C. Nuyts – G. Wain – T. Arts[2]

Turbomachinery and Propulsion Department – "Jacques Chauvin" Laboratory,
von Karman Institute for Fluid Dynamics,
1640 Rhode-Saint-Genèse, Belgium
([1] julien.clinckemaillie@vki.ac.be, [2] tony.arts@vki.ac.be)

ABSTRACT

A detailed analysis of the effect of incoming periodic wakes on the aerodynamic performance of a very-high-lift, mid-loaded low-pressure turbine airfoil (T106C) is presented. This experimental study was performed on a large scale linear cascade in the VKI S-1/C transonic wind tunnel, operating at a fixed exit isentropic Mach number equal to 0.65, covering a range of exit isentropic Reynolds numbers (90,000 – 200,000 based on chord length) and at low inlet free-stream turbulence intensity (0.8 %). The simulation of incoming periodic wakes was realized by means of a disc equipped with bars rotating at high speed upstream of the leading edge plane, allowing an engine representative simulation of the operating conditions (flow coefficient, reduced frequency, wake width and depth) encountered in low-pressure turbines of modern aero-engines. The aerodynamic performance of the airfoil is presented based on measurements performed by means of on-blade static pressure taps, multi-hole probes traversed upstream/downstream of the cascade and on-blade hot-film sensors. Some features of the multi-mode transition germane to unsteady wake-boundary layer interactions in a low-pressure turbine environment are also discussed for specific cases.

NOMENCLATURE

c	Chord
E	Hot-film voltage
f	Frequency
FSTI	Free-stream turbulence intensity
g	Pitch
h	Span
LE	Leading edge
LPT	Low-pressure turbine
M	Mach number
P	Pressure
PS	Pressure side
PSDI	Power spectral density integral
Re	Reynolds number
s	Curvilinear coordinate
SS	Suction side
t	Time
TE	Trailing edge
U	Peripheral speed
V	Velocity
x	Axial coordinate
y	Pitch-wise coordinate

Greek symbols

β	Flow angle
γ	Intermittency
	Isentropic exponent
ϕ	Flow coefficient
τ	Pseudo-wall shear stress
ζ	Kinetic energy loss coefficient

Subscripts

0	Total condition
	Zero-flow condition
	Reference length
1	Upstream condition
2	Downstream condition
ax	Axial
bar	Referring to the bars
is	Isentropic
L	Laminar
m	Mid-span
r	Reduced
T	Turbulent
w	Wall

INTRODUCTION

The actual design trend for modern state-of-the-art commercial aero-engines is characterized by an ever-increasing bypass ratio. This, in turn, requires the low pressure turbine (LPT) to provide an increasingly higher power output in order to drive the large fan, without any efficiency penalty. At the same time, the current need to save weight and to reduce production and maintenance costs translates itself into a reduction of the blade count per row and thus increased pitch-to-chord ratios. The combined effect of those design requirements on the low-pressure turbine implies an increased aerodynamic loading per blade, and has led to the development of very-high-lift – and even ultra-high-lift – airfoils. They are characterized by an increased velocity peak level on the suction side, followed by a significant diffusion of the flow along the rear part of the suction side until the trailing edge. The resulting strong adverse pressure gradient can lead to a separation of the boundary layer, particularly under the low Reynolds number conditions which are germane to low pressure turbines of commercial jet engines operating at cruising altitude. These separation bubbles cause a significant degradation of the engine efficiency, particularly open separation bubbles that fail to reattach, resulting in a major loss in aerodynamic efficiency, thrust and flow turning (Mayle, 1991). For large commercial aero-engines, a component efficiency drop of 2 percent can occur between sea-level take-off conditions, where the Reynolds number is of the order of $5 \cdot 10^5$, and high-altitude cruising conditions where the Reynolds number drops by a factor of 3 to 4 (Volino et al., 2001, Hodson et al., 2005). This drop in efficiency can even become as large as 7 percent for smaller engines operating at even higher cruising altitudes (e.g. Unmanned Aerial Vehicles, Hodson et al., 2005). Due to the low Reynolds numbers typical of high-altitude cruising conditions, a large part of the boundary layer developing on the suction surface of a very-high-lift LPT blade may still be laminar until past the velocity peak, even with significant background free-stream turbulence intensity levels. If the subsequent diffusion is strong enough, the boundary layer is not able to withstand the adverse pressure gradient and separates from the surface. If transition from laminar to turbulent occurs soon enough in the separated free shear layer, the flow will reattach to the surface and a separation bubble is formed. The separation and transition of the boundary layer are thus closely linked, and the accurate prediction of transition onset and development under relevant conditions is essential to the design of efficient LPT airfoils.

A considerable wealth of information on transition can be found in the literature. Mayle (1991) discerned three modes of transition and considered that none of them is more crucial to low-pressure turbines than the separated-flow transition mode. A classification of the separated-flow transition based on the type of separation bubble, long or short, and its effect on the overall pressure distribution along the suction surface was also proposed. Short bubbles have only a local displacement effect, with the pressure distribution before and after the bubble remaining very close to that of the flow without separation, whereas long bubbles interact with the outer flow to such an extent that the overall pressure distribution is modified by the different flow situation at the trailing edge resulting in a more open exit flow angle with an unloaded pressure distribution. The change from a short bubble type to a long one is called bursting, and can be triggered by small changes in either Reynolds number or angle of attack. Mayle's study has since then been critically discussed, reviewed and extended by other research groups such as Walker (1993), Hatman et al. (1999) and Volino et al. (2001).

The transition processes described here above can also be strongly affected by the periodic unsteady nature of the flow in gas turbines. Although the periodic unsteadiness can take multiple forms, the present paper focuses entirely on the unsteady blade-wake interactions, as discussed by Halstead et al. (1997) and Mayle (1991).

A great amount of state-of-the-art studies concerning the aerodynamic performance of very-high-lift low-pressure turbine airfoils under uniform and periodic inflow conditions can be found in the literature. However, most studies have been performed in low-speed wind tunnels (Volino et al., 2001, Schobeiri et al., 2004, Stieger et al., 2003) or in high-speed wind tunnels with an unrealistically high flow coefficient (Ciorciari et al., 2014). The aim of the present study is to contribute to the available literature by discussing the aerodynamic performance of a very-high-lift mid-loaded low-pressure

turbine airfoil (T106C) under engine representative conditions in terms of exit Mach and Reynolds number, and including the effects of unsteady blade row interference phenomena on the behavior of the boundary layer along the suction surface of the airfoil providing a realistic reduced frequency and flow coefficient. The background free-stream turbulence intensity was kept at a low level (0.8 %) in order to better highlight the effects of the periodic unsteady blade-wake interactions.

EXPERIMENTAL SETUP

Experimental Facility

The measurement campaign was performed in the high speed S-1/C wind tunnel of the von Karman Institute (Fig. 1a). This continuous closed-loop wind tunnel is driven by a 615 kW axial flow compressor. A cooler maintains the temperature close to atmospheric conditions (~290 K) and dry air is maintained at all conditions. The mass flow can further be regulated with a by-pass valve, while the absolute pressure level inside the test section can be lowered down to ~10,000 Pa by means of a vacuum pump. This implies that the flow through a linear cascade of two-dimensional LPT airfoils can be aerodynamically investigated over a large range of independently adjusted exit isentropic Mach ($M_{2,is}$ = 0.5 – 0.8) and Reynolds numbers ($Re_{2,is}$ = $2 \cdot 10^4$ – $3 \cdot 10^5$ based on a chord c ranging between 0.02 and 0.10 m), allowing to cover a wide range of engine representative operating conditions.

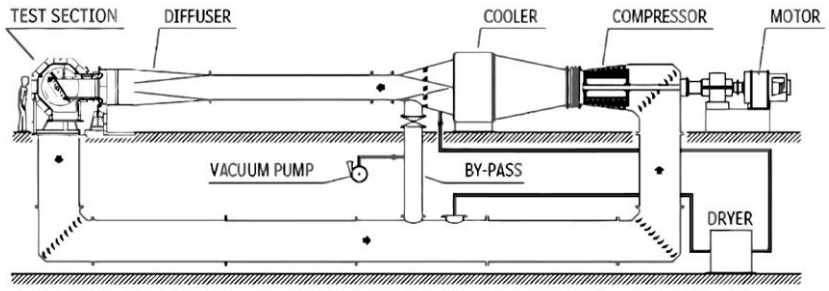

(a) S-1/C wind tunnel

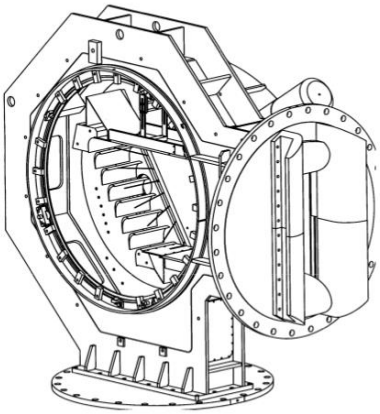

(b) Test section with wake generator

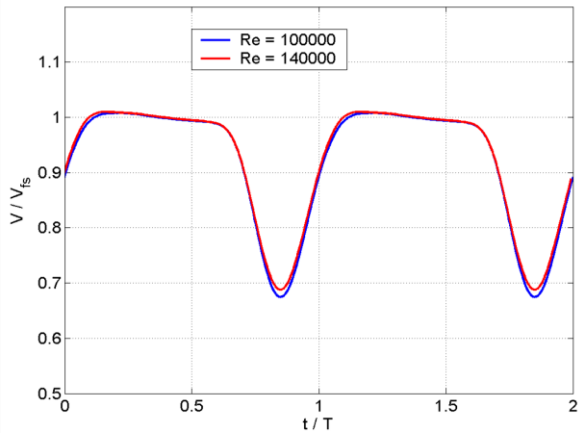

(c) Velocity deficit in the wake (Arts, 2013)

Fig. 1 The S-1/C high speed, variable density wind tunnel

The test section consists of a linear cascade of six up-scaled T106C high-lift, mid-loaded low-pressure turbine blades and two end-blocks (effectively forming 7 blade passages) with a span of 225 mm. This guarantees a sufficiently high aspect ratio (above 2.30) and therewith limits the impact of the end-wall boundary layers at mid-span of the inlet duct. The main characteristics of the test cascade are listed in Tab. 1 (Michálek et al., 2010).

Located in a plane 0.67 x/c_{ax} upstream of the cascade, a spoke-wheel type wake generator equipped with bars and driven by a 30 kW electric motor generates periodically incoming wakes in

order to simulate unsteady blade row interference effects (Fig. 1b and c). The wake generator consists of a solid brass disk with a diameter of 625 mm on which 32 equally spaced cylindrical molybdenum bars with a diameter of 2 mm and a length of 215 mm are mounted. The rotating bars are only parallel to the blade leading edge when passing in front of the central instrumented blade, extending over the entire blade span except for a clearance of 30 mm for safety reasons. The rotational speed of the disk (adjustable by means of a variable frequency controller) as well as the amount of bars were carefully determined in order to match conditions representative of a modern commercial aero-engine in terms of reduced frequency and flow coefficient. For this experimental campaign, a rotational speed of 2,665 RPM was chosen. In this configuration, a flow coefficient $\phi = V_{1,ax}/U_m$ of 0.75 and a reduced frequency $f_r = (f_{bar}\ c)/V_{2,is}$ of 0.62 were achieved. In the following presentation of the results, both cases – uniform (without periodic incoming wakes) and periodic inflow conditions – will be discussed.

Tab. 1 T106C cascade characteristics

Chord	c	mm	93.01
Pitch-to-chord ratio	g/c	-	0.95
Aspect ratio	h/c	-	2.4:1
Blade stagger angle	ϕ	deg	30.7
Inlet flow angle	β_1	deg	32.7
Zweifel (incomp.) = $(2g/c_{ax})\ \cos^2\beta_2\ (\tan\beta_1 - \tan\beta_2)$	Ψ	-	1.29

Instrumentation

The third airfoil from the top of the cascade can be alternatively replaced by an instrumented blade with pneumatic wall static pressure taps or with wall hot-film gauges (for pseudo-wall shear stress measurements). In both cases, the sensors are located at blade mid-span and deployed along the suction side length, with a higher concentration of sensors in the region where the boundary layer is expected to separate at low Reynolds numbers.

A fixed Pitot probe allows measuring the total pressure upstream of the cascade, while the upstream total temperature is quantified by means of a bare type-K thermocouple (without flow velocity correction since the thermocouple is located in a stagnation region). The inlet (P_{01}, T_{01} and β_1) and outlet (P_2) boundary conditions are accurately quantified in measurement planes located at an axial distance of 0.67 x/c_{ax} upstream of the LE and 0.55 x/c_{ax} downstream of the TE respectively. In the presence of the wake generator used to simulate the periodic inflow conditions, the upstream boundary conditions P_{01} and β_1 cannot be measured but are determined using hot-wire data previously obtained in identical flow conditions (Arts et al., 2013) and based on the total pressure measured by a Pitot probe located upstream of the wake generator.

The pitch-wise distributions of flow angle and total pressure upstream and downstream of the cascade were quantified by means of wall static pressure taps, a 3-hole and a 5-hole probe respectively. A Pitot probe with a flattened head was also traversed upstream of the cascade in the span-wise direction in order to characterize the inlet end-wall boundary layer. The latter was quantified as fully turbulent (shape factor = 1.4) with a boundary layer thickness equal to 13% of the inlet duct width and a displacement thickness ranging between 3 and 5 mm for the Reynolds numbers investigated. All pneumatic measurements were sampled at 400 Hz before being subsequently time-averaged, with the exception of the continuous probe traverses which were sampled at 1 kHz with a sufficiently slow carriage speed in order to take into account their relatively low time response.

Since a quantitative calibration of the hot-films array is not possible, the raw output signal of the hot-film gauges was processed in a semi-quantitative manner (Hodson, 1983) using Eq. 1, where the value of the pseudo-wall shear stress is proportional to the associated bridge voltage reading E during the experiment, and the voltage reading E_0 under zero-flow conditions. The hot-film signals were

sampled at 60 kHz and low-pass filtered at 25 kHz. The (measured) frequency response of the hot-film gauges was ~10 kHz.

$$\tau_w = \left(\frac{E^2 - E_0^2}{E_0^2}\right)^3 \quad (1)$$

Uncertainty

The reader should realize that the tests were performed at very low absolute pressure (~10,000 Pa), and that the ambient pressure was used as the main reference pressure for all pneumatic measurements. The application of a rigorous error propagation will therefore lead to higher uncertainties, especially at the lowest Reynolds numbers. However, the obtained results proved to be very repeatable, not only during the measurement campaign, but also when compared to previous measurement campaigns performed in similar flow conditions (Michálek et al., 2010, Arts et al., 2013). The following uncertainty values were estimated for the lowest Reynolds number, the most critical one for the uncertainty estimation. The relative uncertainties on isentropic Mach and Reynolds number are 2.2% and 2.5% respectively, while the absolute uncertainty for the kinetic energy losses and exit flow angle are 0.034 and 1.5 deg respectively.

RESULTS AND DISCUSSION

Time-averaged pneumatic results

Fig. 2 shows the blade velocity evolution (isentropic Mach number evolution) along the suction side of the T106C blade for four exit isentropic Reynolds numbers (90,000 – 200,000), at nominal exit isentropic Mach number (0.65), at low free-stream turbulence intensity (FSTI = 0.8%) and with uniform inflow conditions. The fully turbulent 2D Navier-Stokes numerical computation TRAF2D (using the algebraic Baldwin-Lomax turbulence model, and with uniform inflow boundary conditions) is used as a reference velocity distribution, characterized by a fully attached boundary layer along the entire surface of the airfoil. The reader is referred to Arnone (1994) for more information on the numerical code.

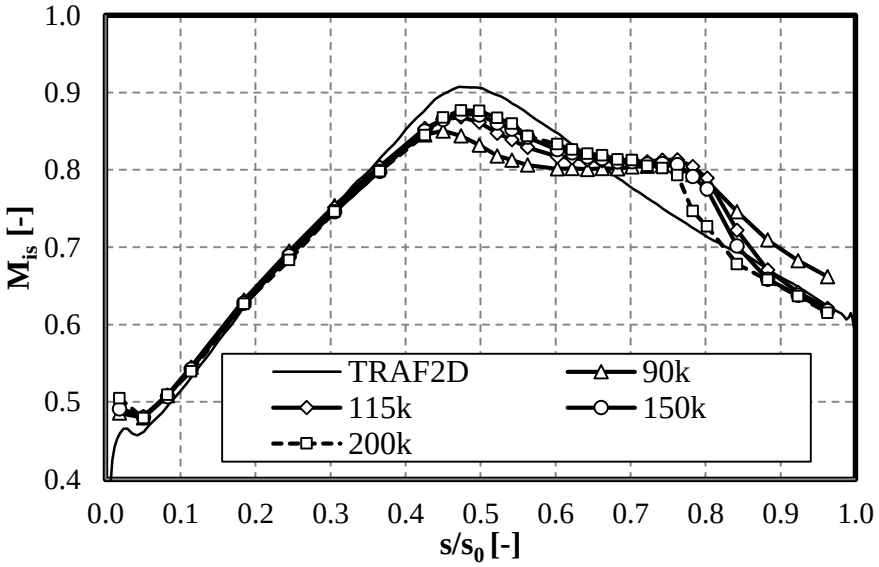

Fig. 2 Isentropic Mach number evolution along the suction side of the T106C blade for four different Reynolds numbers; uniform inflow conditions

For all the investigated cases, the results show a significant deviation from the numerical prediction due to the presence of a separation bubble along the diffusing part of the suction side downstream of the velocity peak. For the highest Reynolds number ($Re_{2,is}$ = 200,000), the separated shear layer is reattaching to the blade surface before the trailing edge, resulting only in a locally perturbed aerodynamic loading of the blade in the region of the separation bubble, caused by the displacement effect of the latter. However, the velocity distribution is significantly altered for the lowest Reynolds number ($Re_{2,is}$ = 90,000) as the separated shear layer is unable to reattach before the trailing edge, resulting in an open separation bubble. Between these two extreme cases, the bursting of the separation bubble from a short type ($Re_{2,is}$ = 150,000) to a long type ($Re_{2,is}$ = 115,000) takes place, corroborating the results obtained by Michálek et al. (2010) which identified a critical Reynolds number of 140,000 at which bubble-bursting takes place.

The mass-averaged kinetic energy losses (Eq. 2) and exit flow angle are presented in Fig. 3, showing the progressive augmentation of losses as well as the reduction in turning angle as the exit isentropic Reynolds number is lowered, culminating in a significant deterioration of the aerodynamic performances for the lowest Reynolds number investigated.

$$\zeta = 1 - \frac{1 - (\overline{P_2}/\overline{P_{02}})^{\gamma-1/\gamma}}{1 - (\overline{P_2}/\overline{P_{01}})^{\gamma-1/\gamma}} \tag{2}$$

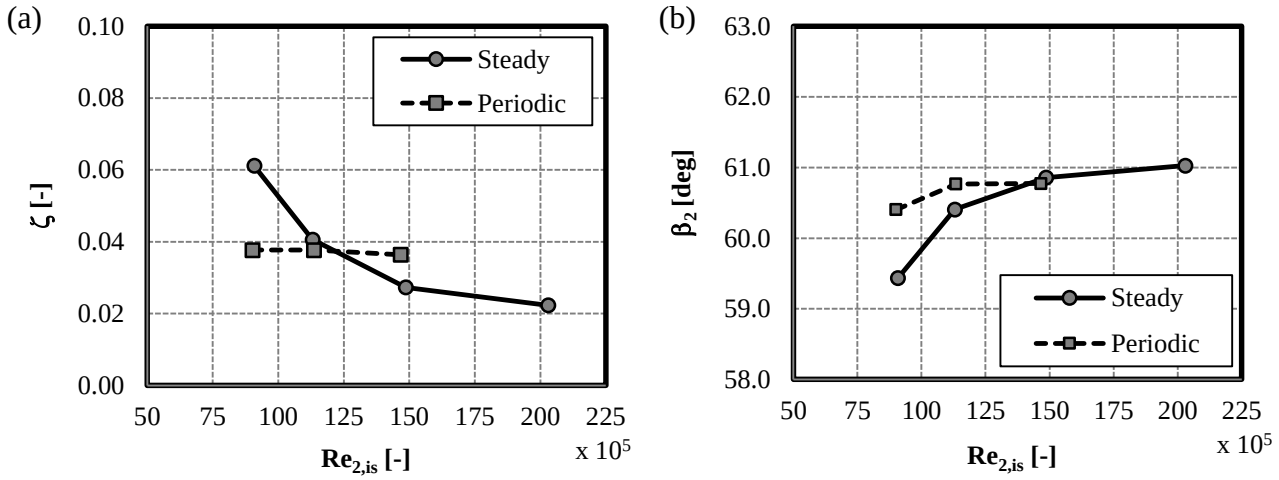

Fig. 3 Mass-averaged kinetic energy losses (a) and exit flow angle (b) as a function of $Re_{2,is}$; comparison between uniform (steady) and periodic inflow conditions

In the presence of periodic incoming wakes generated upstream of the cascade, several conclusions can be drawn from the time-averaged blade velocity distribution alone (Fig. 4) when compared to the results for the lowest Reynolds numbers (90,000 and 115,000) with uniform inflow conditions. The most striking difference compared to the case with uniform inflow conditions is the significant decrease of the separation bubble size even for the lowest Reynolds number. This is due to the reenergizing effect that the convected turbulent wake has on the unstable boundary layer downstream of the velocity peak. A time-averaged reduction of the aerodynamic loading on the front part of the suction surface is also observed, due to the periodically altered inlet velocity triangle in the presence of a wake, resulting therefore in periodic pressure disturbances on the blade surface (Dietz et al., 1992).

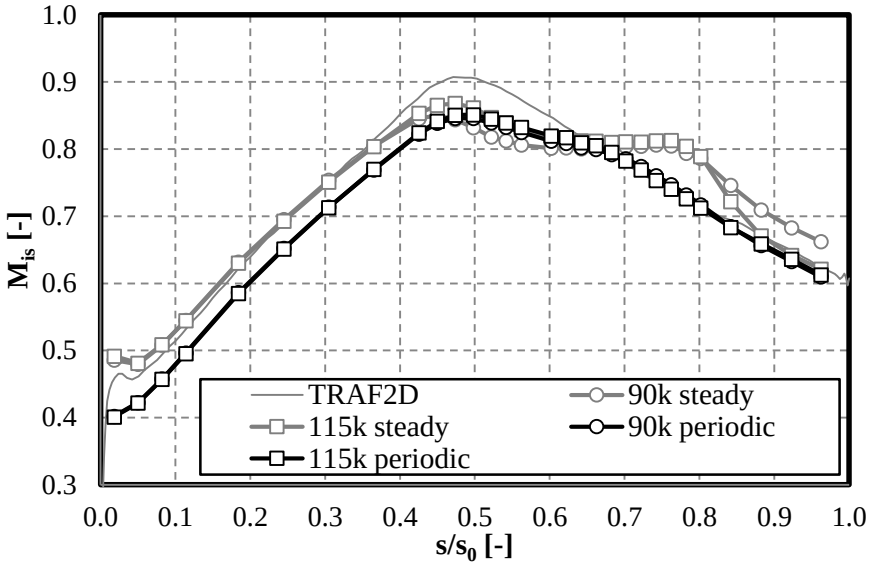

Fig. 4 Isentropic Mach number evolution along the suction side of the T106C blade for two different Reynolds numbers; comparison between uniform (steady) and periodic inflow conditions

Fig. 5 presents the downstream pitchwise traverses through the wake for both uniform (a) and periodic inflow conditions (b). From the uniform case, it is clearly visible that the main source of losses emanates from the suction side of the airfoil since that part of the wake grows wider and deeper with decreasing Reynolds number. Under periodic inflow conditions however, the wake profiles, where P_{01} is an accurate estimation of the inlet total pressure downstream of the wake generator based on previously obtained data (Arts et al., 2013), remain nominally unaltered for different Reynolds numbers, a conclusion that is supported by the relatively constant kinetic energy losses with respect to $Re_{2,is}$ (Fig. 3a). Interestingly, for Reynolds numbers bigger than 125,000, the losses in the periodic case are greater than in the uniform case, an observation that can be attributed to a bigger surface being covered by turbulent flow in the periodic case, thereby increasing the profile losses (Hodson et al., 2005).

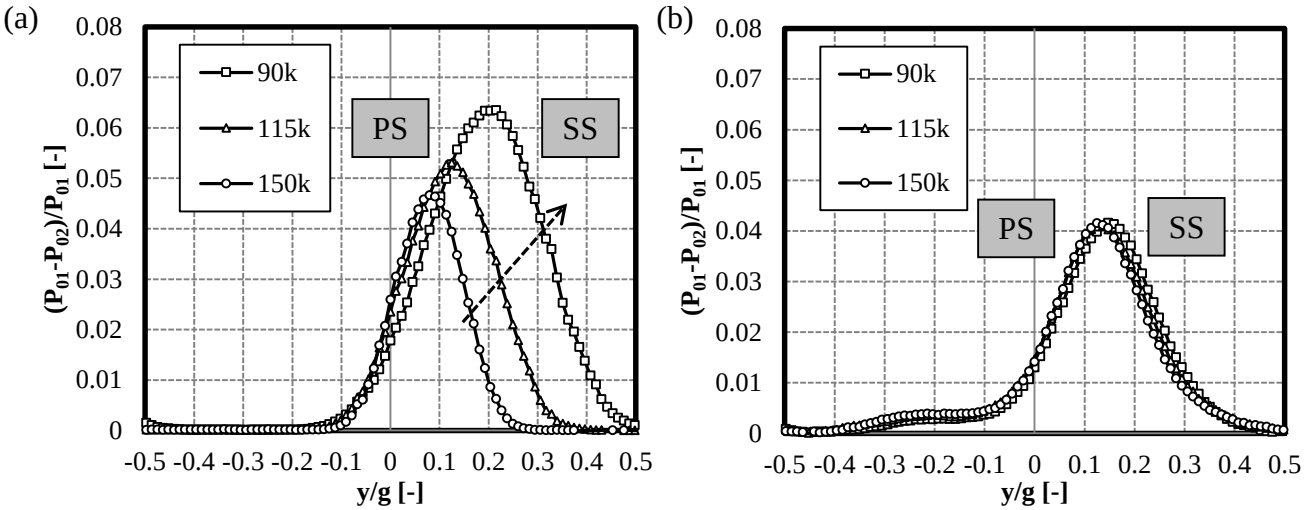

Fig. 5 Pitchwise wake profiles for three different Reynolds numbers; (a) uniform inflow conditions, (b) periodic inflow conditions

Time-resolved hot-films anemometry results

The status of the boundary layer developing on the suction surface of the airfoil can further be investigated using the output signals of hot-film gauges, albeit qualitatively rather than quantitatively

(Eq. 1). Fig. 6a presents the evolution of the mean pseudo-wall shear stress, the rms normalized by the local mean value and the local intermittency factor for one Reynolds number ($Re_{2,is}$ = 115,000) with uniform inflow conditions. The local intermittency factor is computed following Eq. 3 (Coton et al., 2003) and is based on the progressively increasing power spectral density integral (PSDI) throughout the transition process as the boundary layer goes from laminar ($PSDI_L$, γ_{PSDI} = 0) to turbulent ($PSDI_T$, γ_{PSDI} = 1).

$$\gamma_{PSDI(s)} = \frac{PSDI(s) - PSDI_L}{PSDI_T - PSDI_L} \tag{3}$$

Upstream of the velocity peak ($s/s_0 < 0.5$), the pseudo time-averaged wall shear stress values are all above zero with low rms values and a low energy content (Fig. 6b), as expected for an accelerating laminar boundary layer. The spectral peak at ~170 Hz and its first harmonic are believed to be linked to large periodic flow structures generated upstream of the cascade (Michálek et al., 2010). The separation point (s/s_0 = 0.56) is characterized by a zero value for the wall shear stress and a first peak in the rms value as well as a global increase of the energy content, especially in the lower frequency range (1,000 – 2,000 Hz). An explanation for the first peak in rms was proposed by Michálek et al. (2010) who linked it with the periodic ejection of flow from the near-wall region into the shear layer, as described by Hatman and Wang (1999). The high value of the first rms peak can also partly stem from the near-zero mean value of the pseudo-wall shear stress with which the rms is normalized.

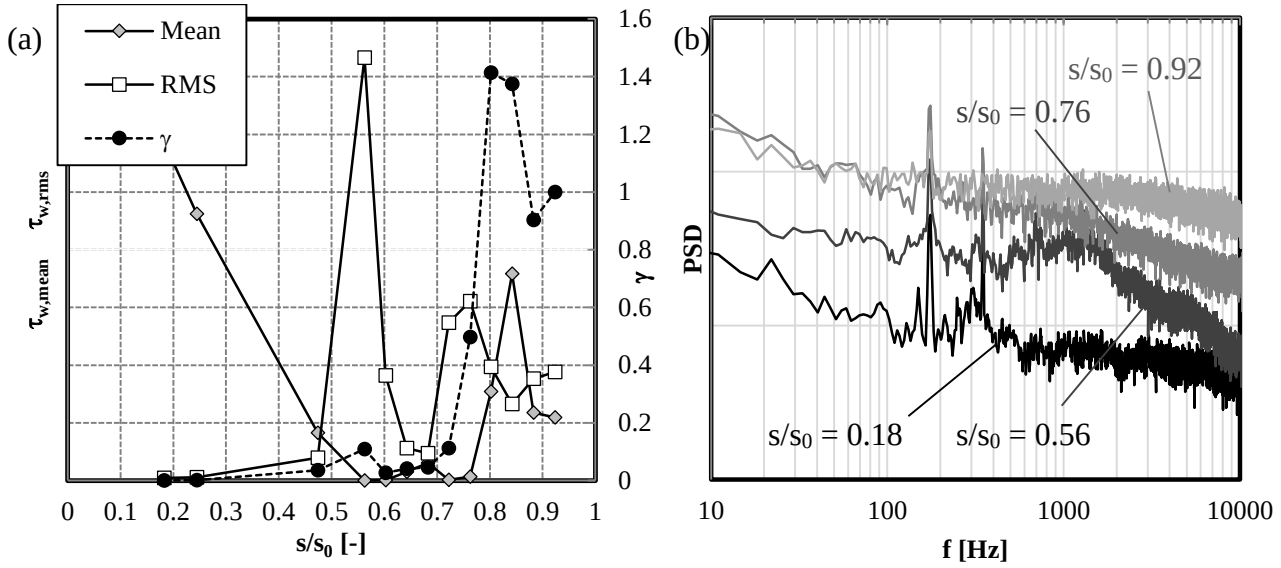

Fig. 6 (a) Pseudo-wall shear stress, the rms and the intermittency factor evolution along the suction side; (b) Power spectral density of four hot-film sensors along the suction side; $Re_{2,is}$ = 115,000; uniform inflow conditions

In the separation region (s/s_0 = 0.64 – 0.68), a slight increase of the wall shear stress can be observed, suggesting the back flow caused by the vortical structure inside the bubble. The transition onset takes place at s/s_0 = 0.68, marked by the gradual increase of both the rms and the local intermittency. The second peak in rms (s/s_0 = 0.76) corresponds to the mid-transition point and the maximum displacement point from the pneumatic measurements. Finally, the end of transition takes place at s/s_0 = 0.84 (just before reattachment), aft of which a fully turbulent boundary layer develops until the trailing edge.

Fig. 7 presents the space-time diagrams of the phase-locked averaged pseudo-wall shear stress (a) and its rms (b) normalized by the maximum value at the same sensor location, thus emphasizing the periodic fluctuation of the signal at the expense of its absolute value, for one Reynolds number

($Re_{2,is}$ = 115,000) and with periodic inflow conditions. Three wake passing events are shown in order to provide a better interpretation of the results. The following discussion concentrates mainly on the diffusing region of the blade ($s/s_0 > 0.5$), where the unsteady wake-boundary layer interaction effects are the most critical.

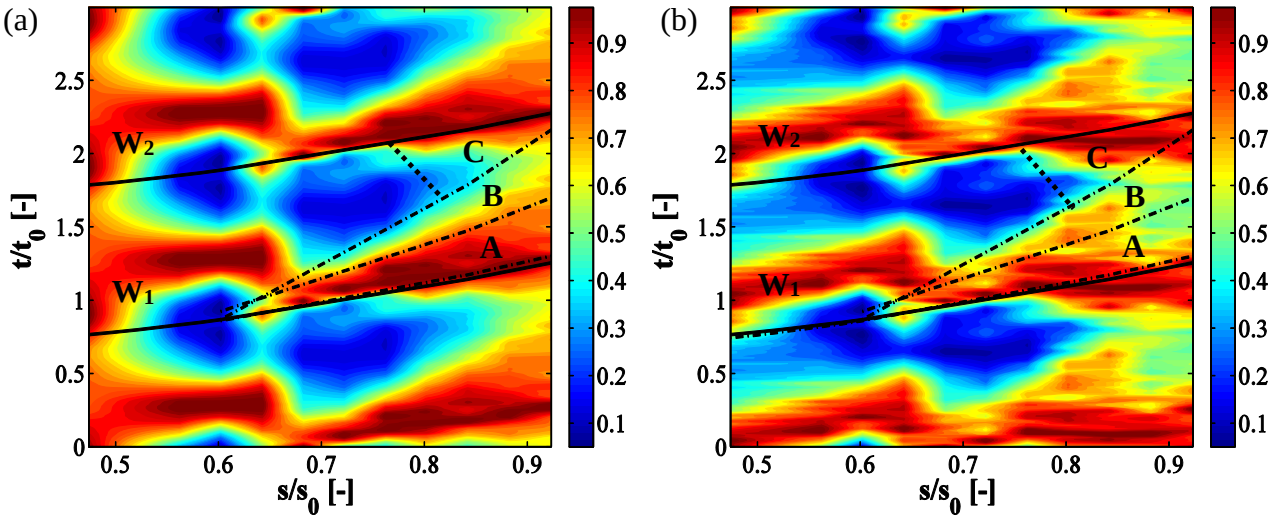

Fig. 7 Space-time diagrams of the phase-locked averaged pseudo-wall shear stress (a) and rms (b) for $Re_{2,is}$ = 115,000; periodic inflow conditions

As described by Halstead et al. (1997), the unsteady boundary layers are developing along two separate but coupled paths: the wake-induced path (lying under the wake trajectory, or lagging slightly behind the latter) and the path between two consecutive wakes.

The first path W_1 induced by the presence of the wake can be clearly observed in the obtained results, with the typical wedge-shaped wake-induced transitional strip (zone A) and the associated calmed region (zone B) starting at the location s/s_0 = 0.62, well into the diffusing part of the blade. The shape of the wedge is related to the different convection velocities of the leading and trailing edges of turbulent spots (0.5 V_{is} and 0.88 V_{is} respectively) as well as the convection velocity of the calmed region (0.3 V_{is}). This transitional region is characterized by an abrupt increase of the wall shear stress coupled with high rms values, followed by a gradual decay of both in the calmed region, an observation that was confirmed by analyzing the hot-film time traces (not shown). In the path between two consecutive wakes, a region of attached (non-zero wall shear stress) transitional (high rms) flow can be observed where the calmed region becomes weaker (zone C), eventually merging with the following wake-induced transitional strip W_2 until the trailing edge. Finally, after analyzing the signal of the most aft hot film sensor, the calmed region could not be discerned anymore, thus assuming that the boundary layer is fully turbulent and attached when reaching the trailing edge of the blade. This is a typical case of multi-mode transition where, at a fixed moment in time, transition can take place at different locations on the blade and be triggered by different mechanisms.

As a final remark, it should be noted that separation, characterized by near-zero wall shear stress and rms values, only seems to take place intermittently between two consecutive wake passing events, an observation that was confirmed after analyzing the time traces of the processed hot-film signals. This demonstrates the overall suppressing effect that incoming wakes have on the separation bubble. The earliest point of separation (s/s_0 = 0.56) also coincides with the separation location under uniform inflow conditions (Fig. 6a).

CONCLUSIONS

A rigorous investigation of the aerodynamic performance of the very-high-lift mid-loaded T106C LPT blade was performed at high isentropic exit Mach number (0.65) and for a range of engine representative isentropic exit Reynolds numbers (90,000 – 200,000), covering the bursting of the separation bubble from a short type to a long or even fully open one.

In the case of uniform inflow conditions, the Reynolds number has a significant influence on the physical size of the separation bubble, and therefore on the aerodynamic losses and loading of the airfoil. A significant deterioration of the aerodynamic performance was observed as the Reynolds number decreases, culminating in a fully open separation bubble at the lowest Reynolds number investigated.

In the case of periodic inflow conditions, a beneficial effect of the unsteady wake-boundary layer interactions was observed at the lower Reynolds numbers (90,000 – 115,000), as the impinging turbulent wakes are periodically suppressing the separation bubble. An analysis of the boundary layer evolution along the diffusing part of the suction surface showed that its development occurs along two distinct paths for one wake-passing event: the wake-induced transitional strip, characterized by its wedge shape and the calmed region, and the path between two consecutive wakes, characterized by attached transitional flow. Furthermore, at higher Reynolds numbers ($Re_{2,is}$ > 125,000), an inversion of the loss evolution occurs: the aerodynamic losses under periodic inflow conditions become more significant than under uniform inflow conditions due to an increased surface being covered by turbulent flow, therefore increasing the profile losses.

ACKNOWLEDGEMENTS

The funding of this work by the Fonds pour la Formation à la Recherche dans l'Industrie et dans l'Agriculture (FRIA - FNRS) is gratefully acknowledged by the first author. The author also wishes to acknowledge the permission to have access to previous experimental results obtained within the framework of the European research projects UTAT (GRD1-2001-40192) and TATMo (AST5-2006-030939) performed at the von Karman Institute. These previously obtained results were solely used as a reference with which the new measurements presented in this paper were compared.

REFERENCES

Arnone, A. (1994). *Viscous analysis of a three-dimensional rotor flow using a multigrid method*. Journal of Turbomachinery, 116:435-445.

Arts, T. (2013). *Aerodynamic performance of two very high lift low pressure turbine airfoils (T106C – T2) at low Reynolds and high Mach numbers*. 5th European Conference for Aerospace Sciences, Munich, Germany.

Ciorciari, R., Kirik, I. and Niehuis, R. (2014). *Effects of Unsteady Wakes on the Secondary Flows in the Linear T106 Turbine Cascade*. Journal of Turbomachinery, 136:091010-1 – 11.

Coton, T., Arts, T., Lefèbvre, M. and Liamis, N. (2003). Unsteady and calming effects investigation on a very high-lift LP turbine blade – Part I: experimental analysis. Journal of Turbomachinery, 125:281-289.

Dietz, A. J., Ainsworth, R. W. (1992). *Unsteady Pressure Measurements on the Rotor of a Model Turbine Stage in a Transient Flow Facility*. ASME 92-GT-156.

Halstead, D. E., Wisler, D. C., Okiishi, T. H., Walker, G. J., Hodson, H. P. and Shin, H.-W. (1997). *Boundary layer development in axial compressors and turbines: part 1 of 4 – Composite picture*. Journal of Turbomachinery, 119:114-127.

Hatman, A. and Wang, T. (1999). *A prediction model for separated-flow transition*. Journal of Turbomachinery, 121:594-602.

Hodson, H. P. and Howell, R. J. (2005). *The role of transition in high-lift low-pressure turbines for aeroengines*. Progress in Aerospace Sciences, 41:419-454.

Hodson, H. P. (1983). *Detection of boundary layer transition and separation in high speed turbine cascades*. Measurement Techniques for Transonic and Supersonic Flow – Proc. 7th Symposium, RWTH Aachen, Germany, pp. 5-1/20.

Mayle, R. E. (1991). *The Role of Laminar-Turbulent Transition in Gas Turbine Engines*. Journal of Turbomachinery, 113:509-537.

Michálek, J., Monaldi, M. and Arts, T. (2010). *Aerodynamic Performance of a Very High Lift Low Pressure Turbine Airfoil (T106C) at Low Reynolds and High Mach Number with Effect of Free Stream Turbulence Intensity*. ASME Turbo Expo 2010: Power for Land, Sea and Air, GT2010-22884, Glasgow, UK.

Schobeiri, M. T., Öztürk, B. (2004). *Experimental Study of the Effect of Periodic Unsteady Wake Flow on Boundary Layer Development, Separation, and Re-Attachment along the Surface of a Low Pressure Turbine Blade*. ASME Turbo Expo 2004: Power for Land, Sea and Air, GT2004-53929, Vienna, Austria.

Stieger, R., Hollis, D., Hodson, H. (2003). *Unsteady Surface Pressures due to Wake Induced Transition in a Laminar Separation Bubble on a LP Turbine Cascade*. ASME Turbo Expo 2003: Power for Land, Sea and Air, GT2003-38303, Atlanta, USA.

Volino, R. J. and Hultgren, L. S. (2001). *Measurements in separated and transitional boundary layers under low-pressure turbine airfoil conditions*. Journal of Turbomachinery, 123:189-197.

Walker, G. J. (1993). *The role of laminar-turbulent transition in gas turbine engines: a discussion*. Journal of Turbomachinery, 115:207-217.